Sio-Iong Ao · Len Gelman
Haeng Kon Kim *Editors*

Transactions on Engineering Technologies

25th World Congress on Engineering (WCE 2017)

Springer

Transactions on Engineering Technologies

Sio-Iong Ao · Len Gelman
Haeng Kon Kim
Editors

Transactions on Engineering Technologies

25th World Congress on Engineering (WCE 2017)

Springer

Editors
Sio-Iong Ao
International Association of Engineers
Hong Kong
Hong Kong

Len Gelman
School of Computing and Engineering
The University of Huddersfield
Queensgate, Huddersfield
UK

Haeng Kon Kim
Department of Computer and Communication
Engineering College, Catholic University of DaeGu
DaeGu
Korea (Republic of)

ISBN 978-981-13-0745-4 ISBN 978-981-13-0746-1 (eBook)
https://doi.org/10.1007/978-981-13-0746-1

Library of Congress Control Number: 2018943704

This Springer imprint is published by the registered company Springer Nature Singapore Pte Ltd.
The registered company address is: 152 Beach Road, #21-01/04 Gateway East, Singapore 189721, Singapore

Preface

A large international conference on Advances in Engineering Technologies and Physical Science was held in London, UK, July 5–7, 2017, under the World Congress on Engineering 2017 (WCE 2017). The WCE 2017 is organized by the International Association of Engineers (IAENG); the Congress details are available at: http://www.iaeng.org/WCE2017. IAENG is a nonprofit international association for engineers and computer scientists, which was founded originally in 1968. The World Congress on Engineering serves as good platforms for the engineering community to meet with each other and to exchange ideas. The conferences have also struck a balance between theoretical and application development. The conference committees have been formed with over three hundred committee members who are mainly research center heads, faculty deans, department heads, professors, and research scientists from over 30 countries. The congress is truly global international event with a high level of participation from many countries. The response to the Congress has been excellent. There have been more than six hundred manuscript submissions for the WCE 2017. All submitted papers have gone through the peer review process, and the overall acceptance rate is 51%.

This volume contains thirty revised and extended research articles written by prominent researchers participating in the conference. Topics covered include mechanical engineering, engineering mathematics, computer science, knowledge engineering, electrical engineering, wireless networks, and industrial applications. The book offers the state of the art of tremendous advances in engineering technologies and physical science and applications, and also serves as an excellent reference work for researchers and graduate students working on engineering technologies and physical science and applications.

Hong Kong, Hong Kong — Sio-Iong Ao
Queensgate, UK — Len Gelman
DaeGu, Korea (Republic of) — Haeng Kon Kim

Contents

Homogenization of Electromagnetic Fields Propagation in a Composite

Helene Canot and Emmanuel Frenod

Abstract In this paper we study the two-scale behavior of the electromagnetic field in 3D in a composite material. It is the continuation of the paper (Canot and Frenod Method of homogenization for the study of the propagation of electromagnetic waves in a composite 2017) [7] in which we obtain existence and uniqueness results for the problem, we performed an estimate that allows us to approach homogenization. Techniques of asymptotic expansion and two-scale convergence are used to obtain the homogenized problem. We justify the two-scale expansion numerically in the second part of the paper.

Keywords Asymptotic Expansion · Electromagnetism · Finite element Harmonic Maxwell Equations · Homogenization · Simulations · Two-scale Convergence

1 Introduction

We are interested in the time-harmonic Maxwell equations in and near a composite material with boundary conditions modeling electromagnetic field radiated by an electromagnetic pulse (EMP). We recall that composite material is composed by carbon fibers periodically enclosed in an epoxy resin which is charged with nanoparticles. In the first part, we have presented the model and proved the existence of a unique solution of the problem. Our mathematical context is periodic

H. Canot (✉) · E. Frenod
Helene Canot and Emmanuel Frenod are in the Department of Mathematics of University of Bretagne Sud (LMBA), Centre Yves Coppens, Bat. B, 1er et., Campus de Tohannic BP 573, 56017 Vannes, France
e-mail: helene.canot@univ-ubs.fr

E. Frenod
e-mail: emmanuel.frenod@univ-ubs.fr

S.-I. Ao et al. (eds.), *Transactions on Engineering Technologies*,
https://doi.org/10.1007/978-981-13-0746-1_1

homogenization. We consider a microscopic scale ε, which represents the ratio between the diameter of the fiber and thickness of the composite material. So, we are trying to understand how the microscopic structure affects the macroscopic electromagnetic field behavior. Homogenization of Maxwell equations with periodically oscillating coefficients was studied in many papers. N. Wellander homogenized linear and non-linear Maxwell equations with perfect conducting boundary conditions using two-scale convergence in [19, 20]. N. Wellander and B. Kristensson homogenized the full time-harmonic Maxwell equation with penetrable boundary conditions and at fixed frequency in Wellander and Kristensson [21]. The homogenized time-harmonic Maxwell equation for the scattering problem was done in Guenneau et al. [11]. Y. Amirat and V. Shelukhin perform two-scale homogenization time-harmonic Maxwell equations for a periodical structure in Amirat and Shelukhin [4]. They calculate the effective dielectric ε and effective electric conductivity σ. They proved that homogenized Maxwell equations are different in low and high frequencies. In our model, we use the Asymptotic expansion suggested by Bensoussan et al. [6] and we justify rigorously mathematical problem by using the theory of two-scale convergence introduced by Nguetseng [15] and developed by Allaire [2]. The result obtained by two-scale convergence approach takes into account the characteristic sizes of skin thickness and wavelength around the material. Then we compare numerically the theoretical result with the homogenized model. The goal is to validate the homogenized procedure for *epsilon* $= 0.01$. The paper was presented at the World Congress on Engineering in London [13].

2 Homogenization

We recall that our problem is:

$$\nabla\times\nabla\times E^\varepsilon - \omega^2\varepsilon^5 k(\varepsilon)E^\varepsilon + i\omega[(\mathbf{1}_C^\varepsilon(\frac{\mathbf{x}}{\varepsilon}) + \varepsilon^4\mathbf{1}_R^\varepsilon(\frac{\mathbf{x}}{\varepsilon}))]E^\varepsilon = 0, \quad \text{in } \Omega. \tag{1}$$

where for a given set $\mathscr{A}$, $\mathbf{1}_{\mathscr{A}}$ stands for the characteristic function of $\mathscr{A}$ and where $\mathbf{1}_{\mathscr{A}}^\varepsilon(\mathbf{x}) = \mathbf{1}_{\mathscr{A}}(\frac{\mathbf{x}}{\varepsilon})$, hence $\mathbf{1}_C^\varepsilon$ and $\mathbf{1}_R^\varepsilon$ are the characteristic functions of the sets filled by carbon fibers and by resin. And where $k(\varepsilon) = (\varepsilon_c\mathbf{1}_C^\varepsilon(\mathbf{x}) + \varepsilon_r\mathbf{1}_R^\varepsilon(\mathbf{x}))$.

Remark 1 We recall that ε_c and ε_r are respectively the relative permittivity of the carbon fibers and the resin. You should not confused with the microscopic scale ε. Equation (1) is provided with the following boundary conditions:

$$\nabla\times E^\varepsilon \times e_2 = -i\omega H_d(x,z)\times e_2 \text{ on } R\times\Gamma_d, \tag{2}$$

and

$$\nabla\times E^\varepsilon \times e_2 = 0 \text{ on } R\times\Gamma_L. \tag{3}$$

We start homogenization approach with the two-scale asymptotic expansion. The rigourous mathematical justification of the homogenized problem was made using two-scale convergence. This concept was introduced by Nguetseng [16] and specified by Allaire [3] which studied properties of the two-scale convergence. Neuss-Radu in [14] presented an extension of two-scale convergence method to the periodic surfaces. Many authors applied two-scale convergence approach Cionarescu and Donato [9], Crouseilles et al. [10], Amirat et al. [1] and also Back and Frénod [5]. This mathematical concept were applied to homogenize the time-harmonic Maxwell equations Ouchetto et al. [17], Pak [18].

In our model, the parallel carbon cylinders are periodically distributed in direction x and z, as the material is homogenous in the y direction, we can consider that the material is periodic with a three directional cell of periodicity. In other words, introducing $\mathscr{Z} = [-\frac{1}{2}, \frac{1}{2}] \times [-1, 0]^2$, function Σ^ε given in Canot and Frenod [8] is naturally periodic with respect to (ξ, ζ) with period $[-\frac{1}{2}, \frac{1}{2}] \times [-1, 0]$ but it is also periodic with respect to $\mathbf{y}$ with period $\mathscr{Z}$.

Now, we review some basis definitions and results about two-scale convergence.

2.1 Two-Scale Convergence

We first define the function spaces

$$\begin{aligned} \mathbf{H}(\text{curl}, \Omega) &= \{u \in \mathbf{L}^2(\Omega) : \ \nabla \times u \in \mathbf{L}^2(\Omega)\}, \\ \mathbf{H}(\text{div}, \Omega) &= \{u \in \mathbf{L}^2(\Omega) : \ \nabla \cdot u \in L^2(\Omega)\}, \end{aligned} \tag{4}$$

with the usual norms:

$$\begin{aligned} \|u\|^2_{\mathbf{H}(\text{curl},\Omega)} &= \|u\|^2_{\mathbf{L}^2(\Omega)} + \|\nabla \times u\|^2_{\mathbf{L}^2(\Omega)}, \\ \|u\|^2_{\mathbf{H}(\text{div},\Omega)} &= \|u\|^2_{\mathbf{L}^2(\Omega)} + \|\nabla \cdot u\|^2_{L^2(\Omega)}. \end{aligned} \tag{5}$$

They are well known Hilbert spaces.

$$\begin{aligned} \mathbf{H}_\#(\text{curl}, \mathscr{Z}) &= \{u \in \mathbf{H}(\text{curl}, R^3) : u \text{ is } \mathscr{Z}\text{-periodic}\} \\ \mathbf{H}_\#(\text{div}, \mathscr{Z}) &= \{u \in \mathbf{H}(\text{div}, R^3) : u \text{ is } \mathscr{Z}\text{-periodic}\} \end{aligned} \tag{6}$$

We introduce

$$\mathbf{L}^2_\#(\mathscr{Z}) = \{u \in \mathbf{L}^2(R^3), u \text{ is } \mathscr{Z}\text{-periodic}\}, \tag{7}$$

and

$$\mathbf{H}^1_\#(\mathscr{Z}) = \{u \in \mathbf{H}^1(R^3), u \text{ is } \mathscr{Z}\text{-periodic}\}, \tag{8}$$

where $\mathbf{H}^1(R^3)$ is the usual Sobolev space on R^3. First, denoting by $\mathbf{C}^0_\#(\mathscr{Z})$ the space of functions in $\mathbf{C}^0(R^3)$ and $\mathscr{Z}$-periodic, $\mathbf{C}^0_0(R^3)$ the space of continuous functions over R^3 with compact support, we have the following definitions:

Definition 1 A sequence $u^\varepsilon(\mathbf{x})$ in $\mathbf{L}^2(\Omega)$ two-scale converges to $u_0(\mathbf{x},\mathbf{y}) \in \mathbf{L}^2(\Omega, \mathbf{L}^2_\#(\mathscr{Z}))$ if for every $V(\mathbf{x},\mathbf{y}) \in \mathbf{C}^0_0(\Omega, \mathscr{C}^0_\#(\mathscr{Z}))$

$$\begin{aligned}\lim_{\varepsilon\to 0} \int_\Omega u^\varepsilon(\mathbf{x}) \cdot V(\mathbf{x}, \mathbf{x}/\varepsilon)\, d\mathbf{x} \\ = \int_\Omega \int_\mathscr{Z} u_0(\mathbf{x},\mathbf{y}) \cdot V(\mathbf{x},\mathbf{y})\, d\mathbf{x} d\mathbf{y}.\end{aligned} \tag{9}$$

Proposition 1 *If $u^\varepsilon(\mathbf{x})$ two-scale converges to $u_0(\mathbf{x},\mathbf{y}) \in \mathbf{L}^2(\Omega, \mathbf{L}^2_\#(\mathscr{Z}))$, we have for all $v(\mathbf{x}) \in C_0(\overline{\Omega})$ and all $w(\mathbf{y}) \in \mathbf{L}^2_\#(\mathscr{Z})$*

$$\begin{aligned}\lim_{\varepsilon\to 0} \int_\Omega u^\varepsilon(\mathbf{x}) \cdot v(\mathbf{x}) w(\tfrac{\mathbf{x}}{\varepsilon})\, d\mathbf{x} \\ = \int_\Omega \int_\mathscr{Z} u_0(\mathbf{x},\mathbf{y}) \cdot v(\mathbf{x}) w(\mathbf{y})\, d\mathbf{x} d\mathbf{y}.\end{aligned} \tag{10}$$

Theorem 1 *(Nguetseng). Let $u^\varepsilon(\mathbf{x}) \in \mathbf{L}^2(\Omega)$. Suppose there exists a constant $c > 0$ such that for all ε*

$$\|u^\varepsilon\|_{L^2(\Omega)} \leq c. \tag{11}$$

Then there exists a subsequence of ε (still denoted ε) and $u_0(\mathbf{x},\mathbf{y}) \in \mathbf{L}^2(\Omega, \mathbf{L}^2_\#(\mathscr{Z}))$ such that:

$$u^\varepsilon(\mathbf{x}) \text{ two-scale converges to } u_0(\mathbf{x},\mathbf{y}). \tag{12}$$

Proposition 2 *Let $u^\varepsilon(\mathbf{x})$ be a sequence of functions in $\mathbf{L}^2(\Omega)$, which two-scale converges to a limit $u_0(\mathbf{x},\mathbf{y}) \in \mathbf{L}^2(\Omega, \mathbf{L}^2_\#(\mathscr{Z}))$.*

Then $u^\varepsilon(\mathbf{x})$ converges also to $u(\mathbf{x}) = \displaystyle\int_\mathscr{Z} u_0(\mathbf{x},\mathbf{y}) d\mathbf{y}$ in $\mathbf{L}^2(\Omega)$ weakly.

Furthermore, we have

$$\lim_{\varepsilon\to 0} \|u^\varepsilon\|_{\mathbf{L}^2(\Omega)} \geq \|u_0\|_{\mathbf{L}^2(\Omega\times Y)} \geq \|u\|_{\mathbf{L}^2(\Omega)}. \tag{13}$$

Proposition 3 *Let $u^\varepsilon(\mathbf{x})$ be bounded in $\mathbf{L}^2(\Omega)$. Up to a subsequence, $u^\varepsilon(\mathbf{x})$ two-scale converges to $u_0(\mathbf{x},\mathbf{y}) \in \mathbf{L}^2(\Omega, \mathbf{L}^2_\#(\mathscr{Z}))$ such that:*

$$u_0(\mathbf{x},\mathbf{y}) = u(\mathbf{x}) + \widetilde{u_0}(\mathbf{x},\mathbf{y}), \tag{14}$$

where $\widetilde{u_0}(\mathbf{x},\mathbf{y}) \in \mathbf{L}^2(\Omega, \mathbf{L}^2_\#(\mathscr{Z}))$ satisfies

$$\int_\mathscr{Z} \widetilde{u_0}(\mathbf{x},\mathbf{y})\, d\mathbf{y} = 0, \tag{15}$$

and $u(\mathbf{x}) = \displaystyle\int_\mathscr{Z} u_0(\mathbf{x},\mathbf{y})\, d\mathbf{y}$ is a weak limit in $\mathbf{L}^2(\Omega)$.

Proof Due to the a priori estimates (32), $u^\varepsilon(\mathbf{x})$ is bounded in $\mathbf{L}^2(\Omega)$, then by application of Theorem 1, u^ε we get the first part of the proposition. Furthermore by defining $\widetilde{u_0}$ as

$$\widetilde{u_0}(\mathbf{x},\mathbf{y}) = u_0(\mathbf{x},\mathbf{y}) - \int\limits_{\mathscr{Z}} u_0(\mathbf{x},\mathbf{y})d\mathbf{y}, \tag{16}$$

we obtain the decomposition (14) of u_0.

Proposition 4 *Let any two-scale limit $u_0(\mathbf{x},\mathbf{y})$, given by Proposition (3), can be decomposed as*

$$u_0(\mathbf{x},\mathbf{y}) = u(\mathbf{x}) + \nabla_{\mathbf{y}}\Phi(\mathbf{x},\mathbf{y}). \tag{17}$$

where $\Phi \in \mathbf{L}^2(\Omega, \mathbf{H}^1_\#(\mathscr{Z}))$ is a scalar-valued function and where $u \in \mathbf{L}^2(\Omega)$.

Proof Proof of (17), integrating by parts, for any $V(\mathbf{x},\mathbf{y}) \in \mathbf{C}^1_0(\Omega, \mathbf{C}^1_\#(\mathscr{Z}))$, we have

$$\begin{aligned}
&\varepsilon \int\limits_{\Omega} \nabla\times u^\varepsilon(\mathbf{x}) \cdot V(\mathbf{x}, \tfrac{\mathbf{x}}{\varepsilon})\, d\mathbf{x} \\
&= \varepsilon \int\limits_{\Omega} u^\varepsilon(\mathbf{x}) \cdot \nabla\times V(\mathbf{x}, \tfrac{\mathbf{x}}{\varepsilon})\, d\mathbf{x} \\
&= \int\limits_{\Omega} u^\varepsilon(\mathbf{x})\{\varepsilon\nabla_{\mathbf{x}} \times V(\mathbf{x}, \tfrac{\mathbf{x}}{\varepsilon}) + \nabla_{\mathbf{y}} \times V(\mathbf{x}, \tfrac{\mathbf{x}}{\varepsilon})\}\, d\mathbf{x}.
\end{aligned} \tag{18}$$

Taking the two-scale limit as $\varepsilon \to 0$ we obtain

$$0 = \int\limits_{\Omega}\int\limits_{\mathscr{Z}} u_0(\mathbf{x},\mathbf{y}) \cdot \nabla_{\mathbf{y}} \times V(\mathbf{x},\mathbf{y})\, d\mathbf{x}d\mathbf{y}, \tag{19}$$

which implies that $\nabla_{\mathbf{y}} \times u_0(\mathbf{x},\mathbf{y}) = 0$. To end the proof of the proposition we use the following result.

Proposition 5 *If $u_0 \in \mathbf{L}^2(\Omega)$ satisfies*

$$\nabla_{\mathbf{y}} \times u_0(\mathbf{x},\mathbf{y}) = 0, \tag{20}$$

then there exists $u \in \mathbf{L}^2(\Omega)$ and $\Phi \in \mathbf{L}^2(\Omega, \mathbf{H}^1_\#(\mathscr{Z}))$ such that $u_0(\mathbf{x},\mathbf{y}) = u(\mathbf{x}) + \nabla_{\mathbf{y}}\Phi(\mathbf{x},\mathbf{y})$.

Applying this proposition we obtain equality (17) ending the proof of Proposition (4).

3 Homogenized Problem

We will explore in this section the behavior of electromagnetic field E^ε using the asymptotic expansion and the two-scale convergence to determine the homogenized problem. We place in the context of the case 6 with $\delta > L$ and $\overline{\omega} = 10^6 \text{rad.s}^{-1}$, then we have $\eta = 5$ and $\Sigma^\varepsilon_a = \varepsilon$, $\Sigma^\varepsilon_r = \varepsilon^4$, $\Sigma^\varepsilon_c = 1$ which gives the following equation:

$$\nabla\times\nabla\times E^\varepsilon - \omega^2\varepsilon^5 k(\varepsilon)E^\varepsilon + i\omega[(\mathbf{1}_C^\varepsilon(\tfrac{\mathbf{x}}{\varepsilon}) + \varepsilon^4\mathbf{1}_R^\varepsilon(\tfrac{\mathbf{x}}{\varepsilon}))\mathbf{1}_{\{y<0\}} + \varepsilon\mathbf{1}_{\{y>0\}}]E^\varepsilon = 0, \tag{21}$$

where for a given set $\mathscr{A}$, $\mathbf{1}_{\mathscr{A}}$ stands for the characteristic function of $\mathscr{A}$ and where $\mathbf{1}_{\mathscr{A}}^\varepsilon(\mathbf{x}) = \mathbf{1}_{\mathscr{A}}(\frac{\mathbf{x}}{\varepsilon})$, hence $\mathbf{1}_C^\varepsilon$ and $\mathbf{1}_R^\varepsilon$ are the characteristic functions of the sets filled by carbon fibers and by resin. And where $k(\varepsilon) = (\varepsilon_c\mathbf{1}_C^\varepsilon(\mathbf{x}) + \varepsilon_r\mathbf{1}_R^\varepsilon(\mathbf{x}))\mathbf{1}_{\{y<0\}} + \mathbf{1}_{\{y>0\}}$. First, we will use the classical method of the asymptotic expansion.

3.1 Asymptotic Expansion

We assume that $(E^\varepsilon, H^\varepsilon)$ satisfies the following asymptotic expansion, as $\varepsilon \to 0$:

$$E^\varepsilon(\mathbf{x}) = E_0(\mathbf{x}, \frac{\mathbf{x}}{\varepsilon}) + \varepsilon E_1(\mathbf{x}, \frac{\mathbf{x}}{\varepsilon}) + \varepsilon^2 E_2(\mathbf{x}, \frac{\mathbf{x}}{\varepsilon}) + ..., \tag{22}$$

where for any $k \in N$ $E_k = E_k(\mathbf{x}, \mathbf{y})$ are considered as $\mathscr{Z}$-periodic functions with respect to $\mathbf{y}$. Applied to functions $E_k(\mathbf{x}, \frac{\mathbf{x}}{\varepsilon})$ the curl operator becomes $\nabla_\mathbf{x} \times E_k(\mathbf{x}, \frac{\mathbf{x}}{\varepsilon}) + \frac{1}{\varepsilon}\nabla_\mathbf{y} \times E_k(\mathbf{x}, \frac{\mathbf{x}}{\varepsilon})$. Plugging (22) in the formulations (21), gathering the coefficients with the same power of ε, we get:

$$\left\{\begin{array}{l}
\frac{1}{\varepsilon^2}\nabla_\mathbf{y}\times\nabla_\mathbf{y}\times E_0(\mathbf{x}, \frac{\mathbf{x}}{\varepsilon}) \\
+\frac{1}{\varepsilon}[\nabla_\mathbf{y}\times\nabla_\mathbf{y}\times E_1(\mathbf{x}, \frac{\mathbf{x}}{\varepsilon}) + \nabla_\mathbf{y}\times\nabla_\mathbf{x}\times E_0(\mathbf{x}, \frac{\mathbf{x}}{\varepsilon}) + \nabla_\mathbf{x}\times\nabla_\mathbf{y}\times E_0(\mathbf{x}, \frac{\mathbf{x}}{\varepsilon})] \\
+\varepsilon^0[\nabla_\mathbf{x}\times\nabla_\mathbf{y}\times E_1(\mathbf{x}, \frac{\mathbf{x}}{\varepsilon}) + \nabla_\mathbf{x}\times\nabla_\mathbf{x}\times E_0(\mathbf{x}, \frac{\mathbf{x}}{\varepsilon}) \\
+\nabla_\mathbf{y}\times\nabla_\mathbf{y}\times E_2(\mathbf{x}, \frac{\mathbf{x}}{\varepsilon}) + \nabla_\mathbf{y}\times\nabla_\mathbf{x}\times E_1(\mathbf{x}, \frac{\mathbf{x}}{\varepsilon}) + i\omega\mathbf{1}_C^\varepsilon(\mathbf{x})\mathbf{1}_{\{y<0\}}E_0(\mathbf{x}, \frac{\mathbf{x}}{\varepsilon})] \\
+\varepsilon[\nabla_\mathbf{x}\times\nabla_\mathbf{y}\times E_2(\mathbf{x}, \frac{\mathbf{x}}{\varepsilon}) + \nabla_\mathbf{x}\times\nabla_\mathbf{x}\times E_1(\mathbf{x}, \frac{\mathbf{x}}{\varepsilon})) + \nabla_\mathbf{y}\times\nabla_\mathbf{x}\times E_2(\mathbf{x}, \frac{\mathbf{x}}{\varepsilon}) \\
+\nabla_\mathbf{y}\times\nabla_\mathbf{y}\times E_3(\mathbf{x}, \frac{\mathbf{x}}{\varepsilon}) + i\omega(\mathbf{1}_C^\varepsilon(\mathbf{x})\mathbf{1}_{\{y<0\}}E_1(\mathbf{x}, \frac{\mathbf{x}}{\varepsilon}) \\
+\mathbf{1}_{\{y>0\}})E_0(\mathbf{x}, \frac{\mathbf{x}}{\varepsilon})] + ...) = 0.
\end{array}\right. \tag{23}$$

In order to write what is in factor of ε in the last equation we used that : $\mathbf{1}_{\{y<0\}} = \mathbf{1}_{\{\frac{y}{\varepsilon}<0\}}$. Since (23) is considered as true for any small ε it gives a cascade of equations, from which we extract the four first equations

$$\left\{\begin{array}{l}
\nabla_\mathbf{y}\times\nabla_\mathbf{y}\times E_0(\mathbf{x}, \mathbf{y}) = 0 \\
\nabla_\mathbf{y}\times\nabla_\mathbf{y}\times E_1(\mathbf{x}, \mathbf{y}) + \nabla_\mathbf{y}\times\nabla_\mathbf{x}\times E_0(\mathbf{x}, \mathbf{y}) + \nabla_\mathbf{x}\times\nabla_\mathbf{y}\times E_0(\mathbf{x}, \mathbf{y}) = 0 \\
\nabla_\mathbf{x}\times\nabla_\mathbf{y}\times E_1(\mathbf{x}, \mathbf{y}) + \nabla_\mathbf{x}\times\nabla_\mathbf{x}\times E_0(\mathbf{x}, \mathbf{y}) + \nabla_\mathbf{y}\times\nabla_\mathbf{y}\times E_2(\mathbf{x}, \mathbf{y}) \\
+\nabla_\mathbf{y}\times\nabla_\mathbf{x}\times E_1(\mathbf{x}, \mathbf{y}) + i\omega\mathbf{1}_C(\mathbf{y})\mathbf{1}_{\{v<0\}}E_0(\mathbf{x}, \mathbf{y}) = 0 \\
\nabla_\mathbf{x}\times\nabla_\mathbf{y}\times E_2(\mathbf{x}, \mathbf{y}) + \nabla_\mathbf{x}\times\nabla_\mathbf{x}\times E_1(\mathbf{x}, \mathbf{y}) \\
+\nabla_\mathbf{y}\times\nabla_\mathbf{x}\times E_2(\mathbf{x}, \mathbf{y}) + \nabla_\mathbf{y}\times\nabla_\mathbf{y}\times E_3(\mathbf{x}, \mathbf{y}) \\
+i\omega\big(\mathbf{1}_C(\mathbf{y})\mathbf{1}_{\{v<0\}}E_1(\mathbf{x}, \mathbf{y}) + \mathbf{1}_{\{v>0\}}\big)E_0(\mathbf{x}, \mathbf{y}) = 0
\end{array}\right. \tag{24}$$

Applying $\mathrm{div}_\mathbf{y}$ in the last two equations in (24), we obtain

$$\nabla_\mathbf{y}\cdot\big(i\omega\mathbf{1}_C(\mathbf{y})\mathbf{1}_{\{v<0\}}E_0(\mathbf{x}, \mathbf{y})\big) = 0, \tag{25}$$

and

$$\nabla_{\mathbf{y}} \cdot \left(i\omega(\mathbf{1}_C(\mathbf{y})\mathbf{1}_{\{\nu<0\}}E_1(\mathbf{x},\mathbf{y}) + \mathbf{1}_{\{\nu>0\}})E_0(\mathbf{x},\mathbf{y}) \right) = 0. \tag{26}$$

The boundary condition in (2) write:

$$\begin{cases} (\frac{1}{\varepsilon}\nabla_{\mathbf{y}} \times E_0(\mathbf{x},\mathbf{y}) + \nabla_{\mathbf{x}} \times E_0(\mathbf{x},\mathbf{y}) + \nabla_{\mathbf{y}} \times E_1(\mathbf{x},\mathbf{y}+...) \times n \\ = -i\omega H_d \times n, \ \mathbf{x} \in \mathbb{R}^3, \ \mathbf{y} \in \mathscr{Z}. \end{cases} \tag{27}$$

Now we take the first equation of (24) and the equation (25) to obtain:

$$\begin{cases} \nabla_{\mathbf{y}} \times \nabla_{\mathbf{y}} \times E_0(\mathbf{x},\mathbf{y}) = 0, \\ \nabla_{\mathbf{y}} \cdot \{i\omega(\mathbf{1}_C(\mathbf{y})\mathbf{1}_{\{\nu<0\}})E_0(\mathbf{x},\mathbf{y})\} = 0. \end{cases} \tag{28}$$

Multiplying the first equation in (28) by E_0 and integrating by parts over $\mathscr{Z}$ leads to

$$\begin{aligned} &\int_{\mathscr{Z}} \nabla_{\mathbf{y}} \times \nabla_{\mathbf{y}} \times E_0(\mathbf{x},\mathbf{y})E_0(\mathbf{x},\mathbf{y}) \ d\mathbf{y} \\ &= \int_{\mathscr{Z}} |\nabla_{\mathbf{y}} \times E_0(\mathbf{x},\mathbf{y})|^2 \ d\mathbf{y} \\ &= 0. \end{aligned} \tag{29}$$

We deduce that the equation is equivalent to

$$\nabla_{\mathbf{y}} \times E_0(\mathbf{x},\mathbf{y}) = 0, \tag{30}$$

for any $\mathbf{y} \in \mathscr{Z}$.

Hence from Proposition (5) we conclude that $E_0(\mathbf{x},\mathbf{y})$ can be decomposed as

$$E_0(\mathbf{x},\mathbf{y}) = E(\mathbf{x}) + \nabla_{\mathbf{y}}\Phi_0(\mathbf{x},\mathbf{y}), \tag{31}$$

where $\Phi_0(\mathbf{x},\mathbf{y}) \in \mathbf{L}^2(\Omega; \mathbf{H}^1_{\#}(\mathscr{Z}))$ and $E(\mathbf{x}) \in \mathbf{L}^2(\Omega)$.

3.2 Mathematical Justification

Now we will show rigorously with two-scale convergence that the solution of problems (1)–(3) converge to the solution of the homogenized problem when ε tends to 0. We recall the following Theorem, we give a proof in Canot and Frenod [8]:

Theorem 2 *For any $\varepsilon > 0$, for any $\eta \geq 0$, there exists a positive constant ω_0 which does not depend on ε and such that for all $\omega \in (0, \omega_0)$, $E^\varepsilon \in X^\varepsilon(\Omega)$ solution of (1)–(3) satisfies*

$$\|E^\varepsilon\|_{\mathbf{X}^\varepsilon(\Omega)} \leq C \tag{32}$$

with $C = \frac{C_{\gamma_t} C_{\gamma_T}}{\mathscr{C}_0} \|H_d\|_{H(curl,\Omega)}$.

Theorem 3 *Under assumptions of Theorem 2, sequence* E^ε *solution of (1)–(3) converges to* $E(\mathbf{x}) \in \mathbf{L}^2(\Omega)$ *which is the unique solution of the homogenized problem:*

$$\begin{cases} \theta_1 \nabla_{\mathbf{x}} \times \nabla_{\mathbf{x}} \times E(\mathbf{x}) + i\omega\theta_2 E(\mathbf{x}) = 0 \ \text{ in } \Omega, \\ \theta_1 \nabla_{\mathbf{x}} \times E(\mathbf{x}) \times e_2 = -i\omega H_d \times e_2 \ \text{ on } \Gamma_d, \\ \nabla_{\mathbf{x}} \times E(\mathbf{x}) \times e_2 = 0 \ \text{ on } \Gamma_L. \end{cases} \tag{33}$$

with $\theta_1 = \int\limits_{\mathscr{Z}} \mathrm{Id} + \nabla_{\mathbf{y}} \chi(\mathbf{y})\, d\mathbf{y}$ *and* $\theta_2 = \int\limits_{\mathscr{Z}} \mathbf{1}_C(\mathbf{y})(\mathrm{Id} + \nabla_{\mathbf{y}} \chi(\mathbf{y}))\, d\mathbf{y}$.

And where the scalar function χ *is the unique solution, up to an additive constant in the Hilbert space of* $\mathscr{Z}$ *periodic functions* $H^1_\#(\mathscr{Z})$*, of the following boundary value problem*

$$\begin{cases} \triangle_{\mathbf{y}}(\chi(\mathbf{y})) = 0 \ \text{ in } \mathscr{Z} \backslash \partial\Omega_C, \\ [\dfrac{\partial \chi}{\partial n}] = -n_j \ \text{ on } \partial\Omega_C, \\ [\chi] = 0 \ \text{ on } \partial\Omega_C. \end{cases} \tag{34}$$

where $[f]$ *is the jump across the surface of* $\partial\Omega_C$, n_j, $j = \{1, 2, 3\}$ *is the projection on the axis* e_j *of the normal of* $\partial\Omega_C$.

Proof **Step 1: Two-scale convergence**. Due to the estimate (32), E^ε is bounded in $\mathbf{L}^2(\Omega)$. Hence, up to a subsequence, E^ε two-scale converges to $E_0(\mathbf{x}, \mathbf{y})$ belonging to $\mathbf{L}^2(\Omega, \mathbf{L}^2_\#(\mathscr{Z}))$. That means for any $V(\mathbf{x}, \mathbf{y}) \in \mathbf{C}^1_0(\Omega, \mathbf{C}^1_\#(\mathscr{Z}))$, we have:

$$\lim_{\varepsilon \to 0} \int\limits_{\Omega} E^\varepsilon(\mathbf{x}) \cdot V(\mathbf{x}, \frac{\mathbf{x}}{\varepsilon})\, d\mathbf{x} = \int\limits_{\Omega} \int\limits_{\mathscr{Z}} E_0(\mathbf{x}, \mathbf{y}) \cdot V(\mathbf{x}, \mathbf{y})\, d\mathbf{y} d\mathbf{x}. \tag{35}$$

Step 2: Deduction of the constraint equation. We multiply the equation (21) by oscillating test function $V^\varepsilon(\mathbf{x}) = V(\mathbf{x}, \frac{\mathbf{x}}{\varepsilon})$ where $V(\mathbf{x}, \mathbf{y}) \in \mathbf{C}^1_0(\Omega, \mathbf{C}^1_\#(\mathscr{Z}))$:

$$\begin{aligned} &\int\limits_{\Omega} \nabla \times E^\varepsilon(\mathbf{x}) \cdot (\nabla_{\mathbf{x}} \times V^\varepsilon(\mathbf{x}, \frac{\mathbf{x}}{\varepsilon}) + \frac{1}{\varepsilon} \nabla_{\mathbf{y}} \times V^\varepsilon(\mathbf{x}, \frac{\mathbf{x}}{\varepsilon})) + [-\omega^2 \varepsilon^5 k(\varepsilon) \\ &\quad + i\omega \big(\big(\mathbf{1}^\varepsilon_C(\frac{\mathbf{x}}{\varepsilon}) + \varepsilon^4 \mathbf{1}^\varepsilon_R(\frac{\mathbf{x}}{\varepsilon}) \big) \mathbf{1}_{\{y<0\}} + \varepsilon \mathbf{1}_{\{y>0\}} \big)] E^\varepsilon \cdot V^\varepsilon(\mathbf{x}, \frac{\mathbf{x}}{\varepsilon})\, d\mathbf{x} \\ &\quad = -i\omega \int\limits_{\Gamma_d} H_d \times e_2 \cdot (e_2 \times V(x, 1, z, \xi, \frac{1}{\varepsilon}, \zeta)) \times e_2\, d\sigma. \end{aligned} \tag{36}$$

Integrating by parts, we get:

$$\begin{aligned}
&\int_{\Omega} E^{\varepsilon}(\mathbf{x}) \cdot (\nabla_{\mathbf{x}} \times \nabla_{\mathbf{x}} \times V^{\varepsilon}(\mathbf{x}, \frac{\mathbf{x}}{\varepsilon}) + \frac{1}{\varepsilon} \nabla_{\mathbf{y}} \times \nabla_{\mathbf{x}} \times V^{\varepsilon}(\mathbf{x}, \frac{\mathbf{x}}{\varepsilon}) \\
&+ \frac{1}{\varepsilon} \nabla_{\mathbf{x}} \times \nabla_{\mathbf{y}} \times V^{\varepsilon}(\mathbf{x}, \frac{\mathbf{x}}{\varepsilon}) + \frac{1}{\varepsilon^2} \nabla_{\mathbf{y}} \times \nabla_{\mathbf{y}} \times V^{\varepsilon}(\mathbf{x}, \frac{\mathbf{x}}{\varepsilon})) + [-\omega^2 \varepsilon^5 k(\varepsilon) \\
&+ i\omega \big(\mathbf{1}_C^{\varepsilon}(\frac{\mathbf{x}}{\varepsilon}) + \varepsilon^4 \mathbf{1}_R^{\varepsilon}(\frac{\mathbf{x}}{\varepsilon})\big) \mathbf{1}_{\{y<0\}} + \varepsilon \mathbf{1}_{\{y>0\}}] E^{\varepsilon}(\mathbf{x}) \cdot V^{\varepsilon}(\mathbf{x}, \frac{\mathbf{x}}{\varepsilon}) \, d\mathbf{x} \\
&= -i\omega \int_{\Gamma_d} H_d \times e_2 \cdot (e_2 \times V(x, 1, z, \xi, \frac{1}{\varepsilon}, \zeta)) \times e_2 \, d\sigma.
\end{aligned} \tag{37}$$

Now we multiply (37) by ε^2 and we pass to the two-scale limit, applying Theorem 1 we obtain:

$$\int_{\Omega} \int_{\mathscr{Z}} E_0(\mathbf{x}, \mathbf{y}) \big(\nabla_{\mathbf{y}} \times \nabla_{\mathbf{y}} \times V(\mathbf{x}, \mathbf{y})\big) \, d\mathbf{y} d\mathbf{x} = 0. \tag{38}$$

We deduce the constraint equation for the profile E_0:

$$\nabla_{\mathbf{y}} \times \nabla_{\mathbf{y}} \times E_0(\mathbf{x}, \mathbf{y}) = 0. \tag{39}$$

Step 3. Looking for the solutions to the constraint equation. Multiplying Equation (39) by E_0 and integrating by parts over $\mathscr{Z}$ leads to

$$\int_{\mathscr{Z}} \nabla_{\mathbf{y}} \times \nabla_{\mathbf{y}} \times E_0(\mathbf{x}, \mathbf{y}) E_0(\mathbf{x}, \mathbf{y}) \; d\mathbf{y} = \int_{\mathscr{Z}} |\nabla_{\mathbf{y}} \times E_0(\mathbf{x}, \mathbf{y})|^2 \; d\mathbf{y} = 0. \tag{40}$$

We deduce that equation (29) is equivalent to

$$\nabla_{\mathbf{y}} \times E_0(\mathbf{x}, \mathbf{y}) = 0, \tag{41}$$

Moreover a solution of (41) is also solution of (39). So (39) and (41) are equivalent.

Hence, from Proposition (17) we conclude that $E_0(\mathbf{x}, \mathbf{y})$ can be decomposed as

$$E_0(\mathbf{x}, \mathbf{y}) = E(\mathbf{x}) + \nabla_{\mathbf{y}} \Phi_0(\mathbf{x}, \mathbf{y}). \tag{42}$$

Step 4. Equations for $E(\mathbf{x})$ and $\Phi_0(\mathbf{x}, \mathbf{y})$. divergence equation of (21) is multiplied with $V(\mathbf{x}, \frac{\mathbf{x}}{\varepsilon}) = \varepsilon v(\mathbf{x}) \psi(\frac{\mathbf{x}}{\varepsilon})$, where $v \in \mathbf{C}_0^1(\Omega)$ and $\psi \in \mathbf{H}_{\#}^1(\mathscr{Z})$. Theorem 1 and integration by parts yields for all $\psi \in \mathbf{H}_{\#}^1(\mathscr{Z})$ and $v \in \mathbf{C}_0^1(\Omega)$

$$
\begin{aligned}
&\lim_{\varepsilon\to 0}\int_{\Omega} \nabla\cdot\{-\omega^2\varepsilon^5 k(\varepsilon)E^\varepsilon(\mathbf{x}) + i\omega[(\mathbf{1}_C^\varepsilon(\frac{\mathbf{x}}{\varepsilon}) + \varepsilon^4\mathbf{1}_R^\varepsilon(\frac{\mathbf{x}}{\varepsilon}))\mathbf{1}_{\{y<0\}} \\
&+ \varepsilon\mathbf{1}_{\{y>0\}}]E^\varepsilon(\mathbf{x})\}\varepsilon v(\mathbf{x})\psi(\frac{\mathbf{x}}{\varepsilon})\, d\mathbf{x} \\
&= -\lim_{\varepsilon\to 0}\int_{\Omega} \{-\omega^2\varepsilon^5 k(\varepsilon)E^\varepsilon(\mathbf{x}) + i\omega[\mathbf{1}_C^\varepsilon(\frac{\mathbf{x}}{\varepsilon}) + \varepsilon^4\mathbf{1}_R^\varepsilon(\frac{\mathbf{x}}{\varepsilon}))\mathbf{1}_{\{y<0\}} \\
&+ \varepsilon\mathbf{1}_{\{y>0\}}]E^\varepsilon\}\cdot(\varepsilon v(\mathbf{x})\psi(\frac{\mathbf{x}}{\varepsilon}) + v(\mathbf{x})\nabla_{\mathbf{y}}\psi(\frac{\mathbf{x}}{\varepsilon}))\, d\mathbf{x} \\
&= -\int_{\Omega}\int_{\mathscr{Z}} v(\mathbf{x})\nabla_{\mathbf{y}}\psi(\mathbf{y})\cdot[i\omega\mathbf{1}_C(\mathbf{y})E_0(\mathbf{x},\mathbf{y})]\, d\mathbf{y}d\mathbf{x} = 0.
\end{aligned}
\tag{43}
$$

from which it follows that

$$
\nabla_{\mathbf{y}}\cdot[i\omega\mathbf{1}_C(\mathbf{y})E_0(\mathbf{x},\mathbf{y})] = 0. \tag{44}
$$

with E_0 given by the decomposition (17). So we obtain the local equation

$$
\nabla_{\mathbf{y}}\cdot[i\omega\mathbf{1}_C(\mathbf{y})\{E(\mathbf{x}) + \nabla_{\mathbf{y}}\Phi_0(\mathbf{x},\mathbf{y})\}]\, d\mathbf{y} = 0. \tag{45}
$$

The potential Φ_0 may be written on the form

$$
\Phi_0(\mathbf{x},\mathbf{y}) = \sum_{j=1}^{3}\chi_j(\mathbf{y})e_j\cdot E(\mathbf{x}) = \chi(\mathbf{y})\cdot E(\mathbf{x}), \tag{46}
$$

From (31) and (46), we get:

$$
E_0(\mathbf{x},\mathbf{y}) = (\mathrm{Id} + \nabla_{\mathbf{y}}\chi(\mathbf{y}))E(\mathbf{x}). \tag{47}
$$

Inserting E_0 in (26) we obtain

$$
\nabla_{\mathbf{y}}\cdot[i\omega\mathbf{1}_C(\mathbf{y})(\mathrm{Id} + \nabla_{\mathbf{y}}\chi(\mathbf{y})] = 0. \tag{48}
$$

Now, we build oscillating test functions satisfying constraint (31) and use them in weak formulation (37). We define test function $V(\mathbf{x},\mathbf{y}) = \alpha(\mathbf{x}) + \nabla_{\mathbf{y}}\beta(\mathbf{x},\mathbf{y})$, $V(\mathbf{x},\mathbf{y}) \in \mathbf{C}_0^1(\Omega, \mathbf{C}_\#^1(\mathscr{Z}))$ and we inject in (37) test function $V^\varepsilon = V(\mathbf{x}, \frac{\mathbf{x}}{\varepsilon})$, which gives:

$$\begin{aligned}
&\int_{\Omega} E^{\varepsilon}(\mathbf{x}) \cdot \big(\nabla_{\mathbf{x}} \times \nabla_{\mathbf{x}} \times V(\mathbf{x}, \frac{\mathbf{x}}{\varepsilon}) + \frac{2}{\varepsilon}\nabla_{\mathbf{x}} \times \nabla_{\mathbf{y}} \times V(\mathbf{x}, \frac{\mathbf{x}}{\varepsilon}) \\
&+ \frac{1}{\varepsilon^2}\nabla_{\mathbf{y}} \times \nabla_{\mathbf{y}} \times V(\mathbf{x}, \frac{\mathbf{x}}{\varepsilon})\big) + [-\omega^2\varepsilon^5 k(\varepsilon) + i\omega(\big(\mathbf{1}_C^{\varepsilon}(\frac{\mathbf{x}}{\varepsilon}) \\
&+ \varepsilon^4 \mathbf{1}_R^{\varepsilon}(\frac{\mathbf{x}}{\varepsilon})\big)\mathbf{1}_{\{y<0\}} + \varepsilon \mathbf{1}_{\{y>0\}})]E^{\varepsilon}(\mathbf{x}) \cdot V(\mathbf{x}, \frac{\mathbf{x}}{\varepsilon})\, d\mathbf{x} \\
&= -i\omega \int_{\Gamma_d} H_d \times e_2 \cdot (e_2 \times V^{\sharp}(x, 1, z, \xi, \zeta)) \times e_2 \, d\sigma,
\end{aligned} \tag{49}$$

with $V(x, 1, z, \xi, \nu, \zeta) = V^{\sharp}(x, 1, z, \xi, \zeta)$ the restriction on V which does not depend on ν. The term containing the constraint, the third one, disappears. Passing to the limit $\varepsilon \to 0$ and replacing the expression of V by the term $\alpha(\mathbf{x}) + \nabla_{\mathbf{y}}\beta(\mathbf{x}, \mathbf{y})$, we have

$$\begin{aligned}
\nabla_{\mathbf{x}} \times \nabla_{\mathbf{y}} \times V(\mathbf{x}, \mathbf{y}) &= \nabla_{\mathbf{x}} \times \nabla_{\mathbf{y}} \times [\alpha(\mathbf{x}) + \nabla_{\mathbf{y}}\beta(\mathbf{x}, \mathbf{y})] \\
&= \nabla_{\mathbf{x}} \times \nabla_{\mathbf{y}} \times (\alpha(\mathbf{x})) + \nabla_{\mathbf{x}} \times \nabla_{\mathbf{y}} \times (\nabla_{\mathbf{y}}\beta(\mathbf{x}, \mathbf{y})) \\
&= \nabla_{\mathbf{x}} \times \nabla_{\mathbf{y}} \times (\nabla_{\mathbf{y}}\beta(\mathbf{x}, \mathbf{y})).
\end{aligned} \tag{50}$$

Since $\nabla_{\mathbf{y}} \times (\nabla_{\mathbf{y}}) = 0$, the term $\frac{2}{\varepsilon}\nabla_{\mathbf{x}} \times \nabla_{\mathbf{y}} \times \nabla_{\mathbf{y}}\beta(\mathbf{x}, \mathbf{y}))$ vanishes. Therefore, (49) becomes:

$$\begin{aligned}
&\int_{\Omega}\int_{\mathscr{Y}} E_0(\mathbf{x}, \mathbf{y}) \cdot \nabla_{\mathbf{x}} \times \nabla_{\mathbf{x}} \times (\alpha(\mathbf{x}) + \nabla_{\mathbf{y}}\beta(\mathbf{x}, \mathbf{y})) \\
&\quad + i\omega \mathbf{1}_C(\mathbf{y}) E_0(\mathbf{x}, \mathbf{y}) \cdot (\alpha(\mathbf{x}) + \nabla_{\mathbf{y}}\beta(\mathbf{x}, \mathbf{y})\, d\mathbf{y}d\mathbf{x} \\
&\quad = -i\omega \int_{\Gamma_d} H_d \times e_2 \cdot (e_2 \times (\alpha(x, 1, z) + \nabla_{\mathbf{y}}\beta(x, 1, z, \xi, \zeta))) \times e_2 \, d\sigma.
\end{aligned} \tag{51}$$

Now in (51) we replace expression E_0 giving by (47). We obtain

$$\begin{aligned}
&\int_{\Omega}\int_{\mathscr{Y}} (\mathrm{Id} + \nabla_{\mathbf{y}}\chi(\mathbf{y}))E(\mathbf{x}) \cdot \big(\nabla_{\mathbf{x}} \times \nabla_{\mathbf{x}} \times (\alpha(\mathbf{x}) + \nabla_{\mathbf{y}}\beta(\mathbf{x}, \mathbf{y})) \\
&\quad + i\omega \mathbf{1}_C(\mathbf{y})(\mathrm{Id} + \nabla_{\mathbf{y}}\chi(\mathbf{y}))E(\mathbf{x})) \cdot (\alpha(\mathbf{x}) + \nabla_{\mathbf{y}}\beta(\mathbf{x}, \mathbf{y}))\, d\mathbf{y}d\mathbf{x} \\
&\quad = -i\omega \int_{\Gamma_d} H_d \times e_2 \cdot (e_2 \times (\alpha(x, 1, z) + \nabla_{\mathbf{y}}\beta(x, 1, z, \xi, \zeta))) \times e_2 \, d\sigma.
\end{aligned} \tag{52}$$

Taking $\alpha(\mathbf{x}) = 0$ in (52), we obtain

$$\int_{\Omega}\int_{\mathscr{Z}} (\mathrm{Id}+\nabla_{\mathbf{y}}\chi(\mathbf{y}))\nabla_{\mathbf{x}}\times\nabla_{\mathbf{x}}\times E(\mathbf{x})\nabla_{\mathbf{y}}\beta(\mathbf{x},\mathbf{y}) + i\omega\mathbf{1}_C(\mathbf{y})(\mathrm{Id}+\nabla_{\mathbf{y}}\chi(\mathbf{y}))E(\mathbf{x})\cdot\nabla_{\mathbf{y}}\beta(\mathbf{x},\mathbf{y})d\mathbf{y}d\mathbf{x}=0. \tag{53}$$

Integrating by parts

$$\int_{\Omega}\int_{\mathscr{Z}} -\nabla_{\mathbf{y}}\cdot\{(\mathrm{Id}+\nabla_{\mathbf{y}}\chi(\mathbf{y}))\nabla_{\mathbf{x}}\times\nabla_{\mathbf{x}}\times E(\mathbf{x})\}\beta(\mathbf{x},\mathbf{y}) - i\omega\nabla_{\mathbf{y}}\cdot\{\mathbf{1}_C(\mathbf{y})(\mathrm{Id}+\nabla_{\mathbf{y}}\chi(\mathbf{y}))E(\mathbf{x})\}\beta(\mathbf{x},\mathbf{y})\,d\mathbf{y}d\mathbf{x}=0. \tag{54}$$

And since $\nabla_{\mathbf{y}}\cdot\{\mathbf{1}_C(\mathbf{y})(\mathrm{Id}+\nabla_{\mathbf{y}}\chi(\mathbf{y}))E(\mathbf{x})\}=0$ we obtain

$$\int_{\Omega}\int_{\mathscr{Z}} -\nabla_{\mathbf{y}}\cdot\{(\mathrm{Id}+\nabla_{\mathbf{y}}\chi(\mathbf{y}))\nabla_{\mathbf{x}}\times\nabla_{\mathbf{x}}\times E(\mathbf{x})\}\beta(\mathbf{x},\mathbf{y})\,d\mathbf{y}d\mathbf{x}=0. \tag{55}$$

which gives the cell problem

$$\nabla_{\mathbf{y}}\cdot[\mathrm{Id}+\nabla_{\mathbf{y}}\chi(\mathbf{y})]=0. \tag{56}$$

From (48) and (56), the scalar function χ is the unique solution, thanks to Lax-Milgram Lemma, up to an additive constant in the Hilbert space of $\mathscr{Z}$ periodic function $H^1_{\#}(\mathscr{Z})$ of the following boundary value problem

$$\begin{cases} \triangle_{\mathbf{y}}(\chi(\mathbf{y}))=0 \ \text{ in } \mathscr{Z}\backslash\partial\Omega_C, \\ [\dfrac{\partial\chi}{\partial n}]=-n_j \ \text{ on } \partial\Omega_C, \\ [\chi]=0 \ \text{ on } \partial\Omega_C. \end{cases} \tag{57}$$

where $[f]$ is the jump across the surface of $\partial\Omega_C$, n_j, $j=\{1,2,3\}$ is the projection on the axis e_j of the normal of $\partial\Omega_C$.

Remark 2 (34) can be seen as an electrostatic problem. Solving (48) and (56) reduces to look for a potential induced by surface density of charges. Then χ is this potential induced by the charges on the interface of carbon fiber.

Setting $\beta(\mathbf{x},\mathbf{y})=0$ in (52) and integrating by parts, we get

$$\int_{\Omega}\int_{\mathscr{Z}} (\mathrm{Id}+\nabla_{\mathbf{y}}\chi(\mathbf{y}))\nabla_{\mathbf{x}}\times\nabla_{\mathbf{x}}\times E(\mathbf{x})\cdot\alpha(\mathbf{x}) + i\omega\mathbf{1}_C(\mathbf{y})(\mathrm{Id}+\nabla_{\mathbf{y}}\chi(\mathbf{y}))E(\mathbf{x})\alpha(\mathbf{x})\,d\mathbf{y}d\mathbf{x} = -i\omega\int_{\Gamma_d} H_d\times e_2\cdot(e_2\times\alpha(x,1,z))\times e_2\,d\sigma. \tag{58}$$

which gives the following well posed problem for $E(\mathbf{x})$

$$\begin{cases} \theta_1 \nabla_{\mathbf{x}} \times \nabla_{\mathbf{x}} \times E(\mathbf{x}) + i\omega\theta_2 E(\mathbf{x}) = 0 \ \text{ in } \Omega, \\ \theta_1 \nabla_{\mathbf{x}} \times E(\mathbf{x}) \times e_2 = -i\omega H_d \times e_2 \ \text{ on } \Gamma_d, \\ \nabla_{\mathbf{x}} \times E(\mathbf{x}) \times e_2 = 0 \ \text{ on } \Gamma_L. \end{cases} \tag{59}$$

with $\theta_1 = \int\limits_{\mathscr{Z}} \mathrm{Id} + \nabla_{\mathbf{y}} \chi(\mathbf{y})\, d\mathbf{y}$ and $\theta_2 = \int\limits_{\mathscr{Z}} \mathbf{1}_C(\mathbf{y})(\mathrm{Id} + \nabla_{\mathbf{y}} \chi(\mathbf{y}))\, d\mathbf{y}$.

This concludes the proof of Theorem (33).

4 Numerical Results

Our goal is to validate the homogenization method by comparing the numerically solution of exact problem (1) with the solution of the homogenized model (33). We solve the problem (1) in Ω with cells of size $\varepsilon = 10^{-2}$. We enter in the software FreeFem ++ [12] the geometry of the problem, the bilinear form and the boundary condition, we perform the computation with Lagrangian P_2 Finite Elements. The numerical results confirm the theoretical study. We start by giving computational parameters that we need in this experiment, for $\varepsilon = 0.01$. The geometry corresponds to the fibers surrounded by resin. The domain is the composite material represented by a colon of carbon fibers in the resin with periodic conditions in the y direction. We compare the direct solution of the adimensioned problem in ε with the homogenized solution. The basic cells in ε periodicity contains a cylinder which the radius is equal to 0.45×10^{-2}m. We take periodic boundary conditions on the right and left sides. In the rescaled system the conductivity began

$$\Sigma^{\varepsilon}(\mathbf{y}) = \Sigma^{\varepsilon}(\xi, \nu, \zeta) = \begin{cases} \Sigma_r^{\varepsilon} = \varepsilon^4 \ \text{ in } \ \Omega_r, \\ \Sigma_c^{\varepsilon} = 1 \ \ \text{ in } \ \Omega_c, \end{cases} \tag{60}$$

The values of the permittivity are $\varepsilon_r = 5$ in the resin part and $\varepsilon_c = 2.5$ in the carbon part. To simplify the calculations, we consider the composite illuminated by a Progressive Monochromatic Plane Wave, propagating in the Oy direction electrically polarized according to Oz, with a normal incidence. The electric field with the carbon fibers in the composite are contained in the xOy plane. Then we use 2D system. On the upper frontier, we consider the oscillating source $H_d = -\exp(-ik_y.y)$ with the constant of propagation which depends on ε, $k_y = \sqrt{(-\omega^2\varepsilon^3 + i\omega\varepsilon^4)}$, and $\omega = 1$. The computations are performed in P_2 Finite Elements and the direct and homogenized solutions are projected on a regular meshes and the number of triangles is 600. In the cell problem the number of triangles is 10368.

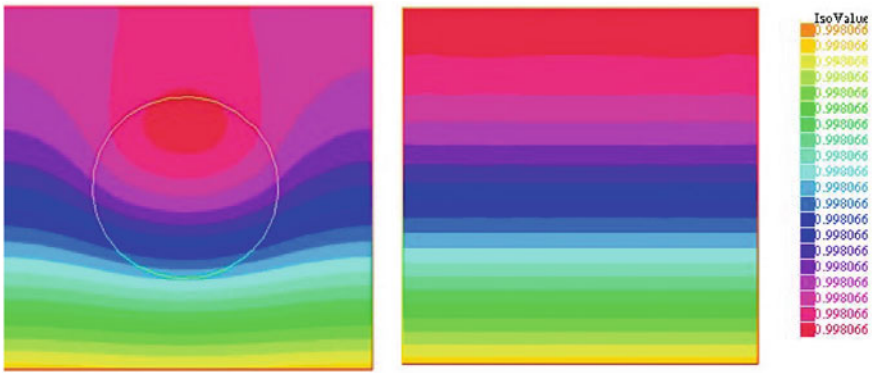

Fig. 1 The z-component of the real part of the electric field E^ε (left) and the homogenized solution (right)

Table 1 The relative error according to the number of fibers

n	Err
2 *fibers*	0.012
10 *fibers*	0.00026
26 *fibers*	0.00013
52 *fibers*	0.00005

4.1 Results of Simulation

In Figure 1, we plot the direct solution of (21), the solution of the homogenized problem without fiber, the transmitted electric field is evaluated. We see that we have no difference between the two approximations. The two solutions represent an attenuated wave propagating along the y-axis. We note that fibers do affect the electromagnetic composite response and our homogenized approach is a good agreement with the exact solution. The decay of the amplitude of the electric field is induced by the imaginary part $\sqrt{i\omega}$ in the carbon fiber and the imaginary part, which depends of ε, $\sqrt{i\omega\varepsilon^4}$ in the resin. To obtain a numerical speed of convergence we compute the relative errors, as εgoes to zero, by increasing the number of the cells and the fibers: $E_{rr} = \frac{\|E^\varepsilon - E(x)\|_{L^2(\Omega)}}{\|E^\varepsilon\|_{L^2(\Omega)}}$ (Table 1).

References

1. Y. Amirat, K. Hamdache , A. Ziani, Homogénéisation d'équations hyperboliques du premier ordre et application aux écoulements missibles en milieux poreux. Ann. Inst. H. Poincaré **6**(5), 397–417 (1989)

2. G. Allaire, Homogenization and two-scale convergence. SIAM J. Math. Anal. **23**(6), 1482–1518 (1992), http://link.aip.org/link/?SJM/23/1482/1. https://doi.org/10.1137/0523084
3. G. Allaire, M. Briand, Multiscale convergence and reiterated homogenization. Proc. Roy. Soc. Edinb. **F126**, 297–342 (1996)
4. Y. Amirat, V. Shelukhin, Homogenization of time-harmonic Maxwell equations and the frequency dispersion effect. J. Maths. Pures. Appl. **95**, 420–443 (2011)
5. A. Back, E. Frenod, Geometric Two-Scale Convergence on Manifold and Applications to the Vlasov Equation. Discrete and Continuous Dynamical Systems - Serie S. Special Issue on Numerical Methods based on Homogenization and Two-Scale Convergence. **8**, 223–241 (2015)
6. A. Bensoussan, J.L. Lions, G. Papanicolaou, Asymptotic analysis for periodic structures, in *Studies in Mathematics and its Applications*, vol. 5 (North Holland, 1978)
7. H. Canot, E. Frenod, Method of homogenization for the study of the propagation of electromagnetic waves in a composite. Part 1: Modeling, Scaling, Existence and Uniqueness Results (2017)
8. H. Canot, E. Frenod, Modeling electromagnetism in and near composite material using two-scale behavior of the time-harmonic Maxwell equations (2016), https://hal.archives-ouvertes.fr/hal-01409522
9. D. Cionarescu, P. Donato, *An Introduction To Homogenization* (Oxford University Press, 1999)
10. N. Crouseilles, E. Frenod, S. Hirstoaga, A. Mouton, Two-Scale Macro-Micro decomposition of the Vlasov equation with a strong magnetic field. Math. Models Methods Appl. Sci. **23**(8), 1527–1559 (2012) (collaboration = CALVI ; IPSO). https://doi.org/10.1142/S0218202513500152, http://hal.archives-ouvertes.fr/hal-00638617/PDF/TSAPSVlas_corr.pdf
11. S. Guenneau, F. Zolla, A. Nicolet. Homogenization of 3D finite photonic crystals with heterogeneous permittivity and permeability. Waves Random Complex Media 653–697 (2007)
12. F. Hecht, O. Pironneau, A. Le Hyaric, FreeFem++ manual (2004)
13. H. Canot, E. Frenod, Method of homogenization for the study of the propagation of electromagnetic waves in a composite part 2: homogenization, in *Lecture Notes in Engineering and Computer Science: Proceedings of The World Congress on Engineering, 5–7 July 2017, London, UK* (2017), pp. 11–15
14. M. Neuss-Radu, Some extensions of two-scale convergence. omptes rendus de l'Academie des sciences. Serie 1 **322**(9), 899–904 (1996)
15. G. Nguetseng, A general convergence result for a functional related to the theory of homogenization. SIAM **20**(3), 608–623 (1989), http://link.aip.org/link/?SJM/20/608/1. https://doi.org/10.1137/0520043?
16. G. Nguetseng, Asymptotic analysis for a stiff variational problem arising in mechanics SIAM J. Math. Anal. **21**(6) 1394–1414 (1990), http://link.aip.org/link/?SJM/21/1394/1. https://doi.org/10.1137/0521078
17. O. Ouchetto, S. Zouhdi, A. Bossavit et al., Effective constitutive parameters of periodic composites, in 2005 European Microwave Conference (IEEE, 2005), p. 2
18. H.E. Pak, Geometric two-scale convergence on forms and its applications to Maxwell's equations, in *2005 European Proceedings of the Royal Society of Edinburgh* vol. 135A, pp. 133–147
19. N. Wellander, Homogenization of the Maxwell equations: case I. Linear Theory Appl. Math. **46**(2), 29–51 (2001)
20. N. Wellander, Homogenization of the Maxwell equations: case II. Nonlinear Cond. Appl. Math. **47**(3), 255–283 (2002)
21. N. Wellander, B. Kristensson, Homogenization of the Maxwell equations at fixed frequency. Technical Report, vol. LUTEDX/TEAT-7103/1-37 (2002)

Statistics of Critical Load in Arrays of Nanopillars on Nonrigid Substrates

Tomasz Derda and Zbigniew Domański

Abstract Multicomponent systems are commonly used in nano-scale technology. Specifically, arrays of nanopillars are encountered in electro-mechanical sense devices. Under a growing load weak pillars crush. When the load exceeds a certain critical value the system fails completely. In this work we explore distributions of such a critical load in overloaded arrays of nanopillars with identically distributed random strength-thresholds (σ_{th}). Applying a Fibre Bundle Model with so-called local load transfer we analyse how statistics of critical load are related to statistics of pillar-strength-thresholds. Based on extensive numerical experiments we show that when the σ_{th} are distributed according to the Weibull distribution, with shape and scale parameters k, and $\lambda = 1$, respectively, then the critical load can be approximated by the same probability distribution. The corresponding, shape and scale, parameters K and Λ are functions of k.

Keywords Array of pillars · Fracture · Load transfer · Scaling · Statistics
Weibull probablity distribution

1 Introduction

Creation and development of new sub-micron scale devices rise questions about reliability of multicomponent systems. One such a question is how performances of individual components combine into a resulting overall performance of the system to which these components belong. This question is important because progressively

T. Derda · Z. Domański (✉)
Institute of Mathematics, Czestochowa University of Technology,
Dabrowskiego 69, PL-42201 Czestochowa, Poland
e-mail: zbigniew.domanski@im.pcz.pl

T. Derda
e-mail: tomasz.derda@im.pcz.pl

S.-I. Ao et al. (eds.), *Transactions on Engineering Technologies*,
https://doi.org/10.1007/978-981-13-0746-1_2

loaded multicomponent systems break when an initial sequence of failures among weakest components develops into an avalanche of failures that may involve all the system components.

Nowadays nanopillar arrays play a crucial role in many areas of technology and science. Photovoltaic devices or grid cells used in experimental biomedicine, to name but a few examples, employ arrays of nanopillars. Fabrication processes of these arrays request a robust transfer of nanopillars between substrates and thus a controllable-fracturing procedure. This is because pillars are detached from the substrate under a suitable-lateral load to ensure a smooth fracturing process.

An effective statistical approach, to study failures in multicomponent systems related to technology, employs Fiber Bundle Models [1–6]. In this work we analyze a set of pillars placed at nodes of a flat-square grid $\mathscr{G}$, and oriented perpendicularly to surface. Pillars imperfections influence strongly the behavior of arrays under load. Due to the imperfections, pillar-strength-thresholds are nonuniform and thus pillars are represented by random load-thresholds (σ_{th}). In our numerical experiments $\left\{\sigma_{th}^{i}\right\}_{i\in\mathscr{G}}$ are quenched random variables distributed according to the Weibull probability distribution function

$$p_{k,\lambda}(\sigma_{th}) = (k/\lambda)(\sigma_{th}/\lambda)^{k-1}\exp[-(\sigma_{th}/\lambda)^{k}] \tag{1}$$

Parameters $k > 0$ and $\lambda > 0$ define the shape and scale of this distribution. Shape parameter k (so-called Weibull index) controls the amount of disorder in the system. We use the Weibull distribution because this probability distribution is very suitable and frequently employed distribution in the context of engineering systems [7, 8].

2 Loading Process and Statistical Modelling

In our approach we consider pillars located on a nonrigid surface that has a non-vanishing compliance. Within this framework the load redistribution turns out to be localized and thus we employ the local load sharing (LLS). Within a short interval between consecutive fractures the load carried by the broken pillar is transferred only to its nearest intact elements. Such a limited-load-range transfer yields non-homogeneous distributions of load. As a consequence regions of stress accumulation appear throughout the system. The growing load on the intact pillars leads to other failures, after which each intact pillar undergoes increasing stress. If the load transfer does not trigger further crushes, a stable configuration emerges meaning that this initial value of F is not sufficient to provoke failure of the entire system, and its value has to be increased by an amount δF. In the simulations we applied a quasi-static loading procedure—if the system is in a stable state the external load is uniformly increased on all the intact pillars just to destroy only the weakest intact pillar.

A sequence of increases in the value of the external load gives F_c which induces an avalanche of failures among all still undestroyed pillars. Application of such a quasi-static loading enable us to determine a minimal load F_c, that is necessary for

destruction of all the pillars. In order to compare results for systems with different numbers of pillars, we scale the critical loads F_c by the initial number of pillars in the system, i.e. we introduce here an intensive quantity, namely $\sigma_c = F_c/N$.

As already mentioned, the pillar-strength-thresholds σ_{th} are drawn from the Weibull distribution (1). Without loss of generality, we assume $\lambda = 1$ and thus the corresponding probability density reads

$$p_{k,1}(\sigma_{th}) = k\sigma_{th}^{k-1} \exp[-\sigma_{th}^{k}] \tag{2}$$

We address a question how these local critical loads distributed according to (2) combine to create an effective-global critical load F_c. Based on our numerical simulations for systems with $N > 100$, we have found that skewnesses of resulting distributions are negative and they decrease with growing N. For this reason we employ two distributions for fitting our skewed data, namely:

1. three-parameter skew normal distribution (SND) [9, 10] defined by

$$p(\sigma_c) = \frac{\exp[-\frac{(\sigma_c-\xi)^2}{2\omega^2}]\mathrm{erfc}[-\frac{\alpha(\sigma_c-\xi)}{\sqrt{2}\omega}]}{\sqrt{2\pi}\,\omega} \tag{3}$$

   where ξ, ω, α are location, scale and shape parameters, respectively.
2. the Weibull distribution:

$$p_{K,\Lambda}(\sigma_c) = (K/\Lambda)(\sigma_c/\Lambda)^{K-1} \exp[-(\sigma_c/\Lambda)^{K}] \tag{4}$$

Studies related to distributions of system's strength in the context of realizations of Fiber Bundle Models are presented in [11–20]. It is worth mentioning that for the GLS rule, σ_c approximately follows the normal distribution, for both the Weibull and uniform distributions of σ_{th}.

3 Results and Discussion

Based on the Fibre Bundle Model and local load sharing rule, we developed a program code for the simulation of the loading process in two-dimensional nanopillar arrays. Intensive numerical simulations are conducted for systems involving $N = L \times L$ pillars, with L ranging from 8 to 128. We have tuned the amount of pillar-strength-threshold disorder by integer values of k ranging from 2 to 20. In order to get reliable statistics, each simulation was repeated 10^5 times.

Figures 1 and 2 show empirical probability density functions of σ_c for chosen systems. In these plots we have also added fitting lines of skew normal (Fig. 1) and Weibull (Fig. 2) probability density functions with parameters computed from the samples. It can be seen that both of these theoretical distributions are in good agreement with empirical distributions of σ_c. Some more precise information concerning

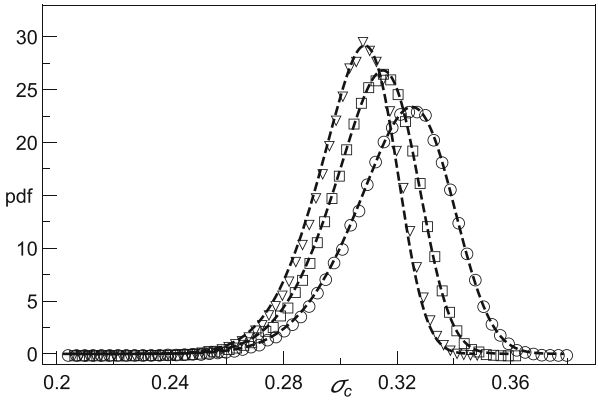

Fig. 1 Empirical probability density functions (pdf) of σ_c for arrays with $L = 64$ (circles), $L = 96$ (squares) and $L = 128$ (triangles). Weibull index $k = 2$ for all presented pdfs. The dashed lines represent skew-normally distributed σ_c with the parameters computed from the simulations

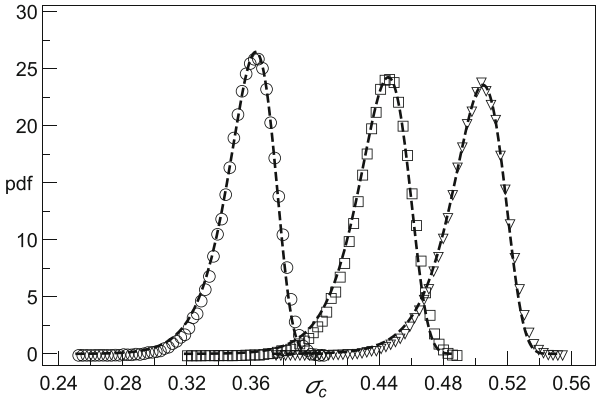

Fig. 2 Empirical probability density functions (pdf) of σ_c for arrays with $L = 128$: $k = 3$ (circles), $k = 5$ (squares) and $k = 7$ (triangles). The dashed lines represent two-parameter Weibull distributed σ_c with the parameters computed from the simulations

the Fig. 2 is gained from a three parameter Weibull distribution, i.e. from an extension of (4) which includes a so-called location parameter. The corresponding cumulative distribution functions reads:

$$P_{K,\Lambda,\mu}(\sigma_c) = 1 - \exp\left[-\left(\frac{\sigma_c - \mu}{\Lambda}\right)^K\right] \tag{5}$$

In Fig. 3 we present distribution (5) for arrays with different number of pillars. We clearly see the support of $\{\sigma_c\}$, with its onset given by the location parameter μ.

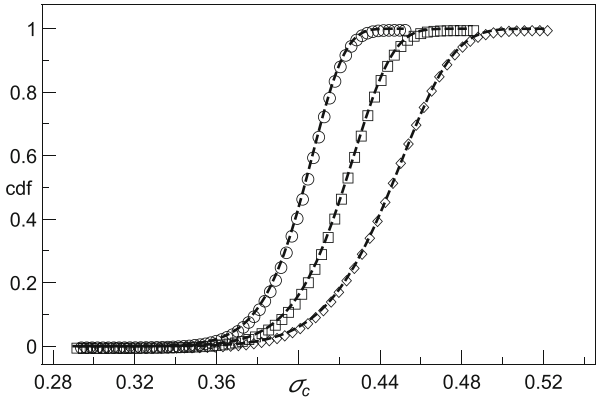

Fig. 3 Empirical cumulative distribution functions (cdf) of σ_c for arrays with $L = 128$ (circles), $L = 64$ (squares) and $L = 32$ (diamonds). Weibull index $k = 4$ for all presented cdfs. The dashed lines represent three-parameter Weibull distributed σ_c with the parameters computed from the simulations

We also present a quantile-quantile plot (Q-Q plot) of the quantiles of the collected data set against the corresponding quantiles given by the SND and Weibull probability distributions. From Figs. 4 and 5, it is seen that the results of fitting by skew normal distribution is slightly better than the Weibull fitting. We also observed that using skew normal distributions give better results than these resulting from two-parameter Weibull fittings. This is true for all analysed systems, especially for the smaller ones. However, it should be noted that the skew normal distribution (3) has one parameter more than two-parameter Weibull distribution (4). Fitting by Weibull distribution allows us to analyse the influence of system properties on the microscopic level (Weibull distributed pillar-strength thresholds) on the macroscopic response (distribution of crical loads) in the framework of one type of distribution. Hence, we focus our attention on the fitting of σ_c distribution by two-parameter Weibull distribution.

In the case of Weibull distribution, values of the fitted parameters K and Λ depend on system size and Weibull index k in the original distribution characterizing the pillar's strength. The plots of the parameters K and Λ are shown in Figs. 6 and 7, respectively. For a fixed value of k, the parameter K is a strictly increasing function of linear system size L. We have found that this relation can be approximated by the following formula

$$K_k(L) = a_1 + a_2\sqrt{L} + a_3 \ln L \tag{6}$$

where a_1, a_2, a_3 are fitted parameters (see page 23). One can also see that fitted curves are (increasingly) ordered according to Weibull index k.

Contrary to K, the parameter Λ is a strictly decreasing function of L, which can be fitted by the formula (see Fig. 7)

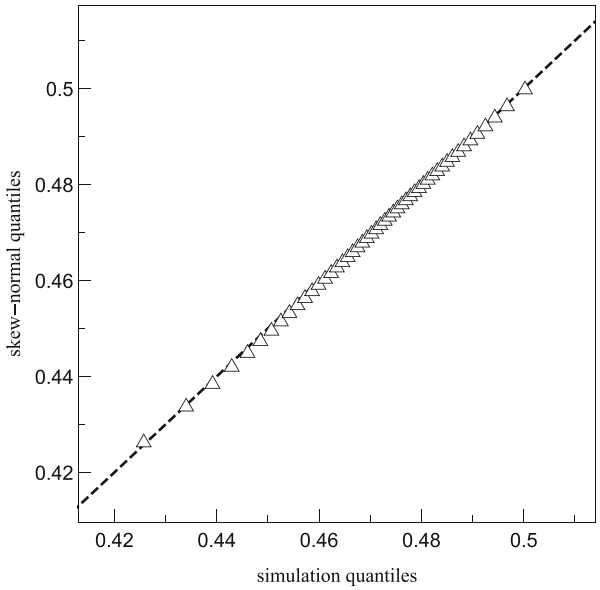

Fig. 4 The Q-Q plot of the quantiles of the set of computed σ_c versus the quantiles of the skew normal distribution. System size $N = 128 \times 128$ and $k = 6$

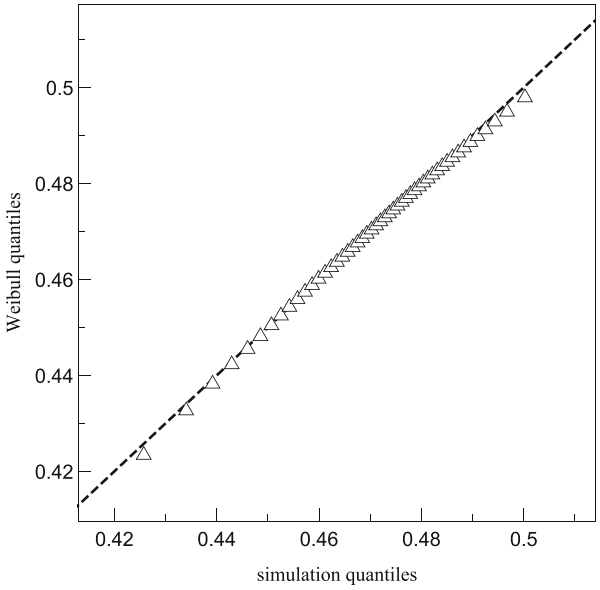

Fig. 5 The Q-Q plot of the quantiles of the set of computed σ_c versus the quantiles of the Weibull distribution. System size $N = 128 \times 128$ and $k = 6$

Weibull index	Fitted parameter		
	a_1	a_2	a_3
$k = 2$	−3.272	−0.200	6.516
$k = 4$	−1.018	−0.454	7.264
$k = 7$	1.742	−0.330	7.446
$k = 10$	3.102	−0.416	8.086
$k = 15$	1.832	−0.927	10.751
$k = 20$	3.268	−0.251	10.218

$$\Lambda_k(L) = b_1 + \frac{b_2}{\sqrt{L}} \tag{7}$$

Weibull index	Fitted parameter	
	b_1	b_2
$k = 2$	0.272	0.440
$k = 4$	0.369	0.470
$k = 7$	0.465	0.490
$k = 10$	0.528	0.492
$k = 15$	0.600	0.482
$k = 20$	0.646	0.484

where b_1, b_2 are matched parameters. The ordering of curves, reported for the previous plot, is preserved.

One of the components of the formula (6) is the natural logarithm of L. If the linear system size is logarithmized, the parameter K can be approximated by the linear function—it is reported in Fig. 8. In turn, Fig. 9 presents values of the parameter Λ in the function of $L^{-1/2}$ which is a part of the function (7). In this case we applied a third degree polynomial as an approximative formula.

Taking assumption that F_c/N follows Weibull distribution with the parameters K and Λ, the expected value of this distribution is given by

$$E[F_c/N] =< F_c/N >= \Lambda\Gamma(1 + \frac{1}{K}) \tag{8}$$

where $\Gamma(1 + \frac{1}{K})$ is the gamma function. From the fitting we have obtained $K \in (9.76, 51.69)$. Substituting limits of this interval into the relation

$$\Gamma(1 + \frac{1}{K})/\Gamma(1) \tag{9}$$

we received two values 0.95 and 0.99. As it was previously mentioned, K is a increasing function of the system size, therefore relation (9) tends to unity with the increasing system size. Consequently, the parameter Λ is a key factor of the formula (8) and the mean critical load can by roughly estimated by